Nanophotonic sensor implants with 3D hybrid periodic-amorphous photonic crystals for wide-angle monitoring of long-term *in-vivo* intraocular pressure

R. H. Siddique[1,2], L. Liedtke[2], H. Park[1,2], S. Y. Lee[3], H. Raniwala[2], D. Y. Park[3], D. H. Lim[3], and H. Choo[2,4]
[1]Image Sensor Lab, Samsung Semiconductor, Inc., Pasadena, USA, email: r.siddique@samsung.com
[2]Caltech, Pasadena, CA, USA, [3] Samsung Medical Center, Seoul, Korea, [4]Samsung Advanced Institute of Technology, Suwon, Korea

2020 IEEE International Electron Devices Meeting (IEDM) | 978-1-7281-8888-1/20/$31.00 ©2020 IEEE | DOI: 10.1109/IEDM13553.2020.9372016

***Abstract*—**Glaucoma, one of the leading cause of irreversible blindness, is largely caused by an elevated intraocular pressure (IOP). However, current IOP monitoring techniques inherit major disadvantages such as imprecision, no real or long time monitoring, and difficult readout. Here, we report on a highly miniaturized (200 um thick) optomechanical nanophotonic sensor implant for long-term, continuous and on-demand IOP monitoring. This IOP sensor is made of a flexible 3D hybrid photonic crystals (HPC) that functions as a pressure-sensitive optical resonator (0.1 nm/mm Hg) and delivers IOP readings when interrogated with near-infrared light with an average accuracy of 0.56 mm Hg over the range of 0–40 mm Hg. A new fabrication process is developed using colloidal self-assembly leading to a single step formation of hybrid periodic and amorphous layers exploiting the inverse process of a drying "coffee-stain" effect. The HPC results in a wide-angle strong resonance of ±40° ensuring an easy and accurate remote and long readout distance. 8 sensors were mounted inside the anterior chamber in New Zealand white rabbits and provided continuous, accurate measurements of IOP with handheld detector for up to 6 months with no signs of inflammation.

I. Introduction

Glaucoma is the leading cause of irreversible blindness after Cataract affecting 79.6 million people worldwide in 2020 [1]. Current clinical therapies aim to lower elevated intraocular pressure (IOP), which is the prime factor for glaucoma progression monitoring and treatment [2]. However, a significant number of patients (over 45%) exhibit some degree of progressive vision loss even after treatment [2]. In addition, an individual's IOP can fluctuate on a daily, weekly, or seasonal basis with various activities, and diet. Therefore, it is crucial to collect regular and comprehensive IOP datasets for physician to predict disease progression and personalize therapy.

In practice, IOP is mostly measured only a few times a year using specialized tonometers with clinical support. The accuracy of the tonometry technology is adversely influenced by variations in individual corneal biomechanics and measurement complexity [3]. Recently, FDA approved contact-lens-based IOP sensors provide continuous for up to 24h, but still indirect and relative IOP measurements by tracking changes in the corneal scleral angle in mV rather than absolute mm [3]. The radio-frequency technology based implants could provide wireless IOP data directly to smartphone. However, their large size compared to eye, short readout distance and fouling complications remain bottleneck for practical solution [3]. Several optical sensing approaches including a fiber-tip-based interferometry for hydrostatic pressure sensing, a pressure-sensitive MEMS structures indentation system show promising results in detecting short-term IOP, however, need further improvements in terms of miniaturization and readout techniques [3]. We have recently demonstrated a miniaturized Fabry-Perot-based optomechanical IOP sensor implants (Dia: 900 µm, Thick: 800 µm) attached on a silicone haptic that overcame the previous issues of ophthalmic implants and provided long-term changes in IOP in awake rabbits over the course of 4.5 months [4,5]. However, the total sensor thickness was still an issue considering the limited space (1.5 - 4 mm) available in the anterior chamber between the iris and innermost membrane (endothelium) of the cornea.

In this work, we have developed a nanophotonic based optomechnical device and reported the smallest IOP implant (Dia: 500 um, Thick: 200 um) that can be placed in any area under the cornea into the anterior chamber without touching the endothelium (Fig. 1a). The sensor is made of only flexible biocompatible silicone/polydimethylsiloxane (PDMS) and structured as 3D hybrid photonic crystal for wide angle (±40°) pressure dependent NIR resonance (0.1 nm/mm Hg) (Fig. 1b) using colloidal lithography and inverse "coffee-stain" effect. Using our IOP-sensing implant and handheld detector system, we have successfully tracked long-term changes in IOP in 8 awake rabbits over the course of 6 months with good consistency in comparison to commercial TonoVet.

II. Results

A. *Design and fabrication of nanophotonic IOP sensor*

The implantable IOP sensor is made of sponge-like spherical air voids within medical grade silicone/PDMS arranged in an amorphous pattern at the top and face-cubic periodic pattern at the bottom half as shown in the scanning electron images (SEM) in Fig. 2. The fabrication flow is shown in the schematics in Fig. 3. First, a droplet of polystyrene colloidal solution is poured onto a hydrophobic monolayer-coated substrate and heated at 50°C to self-assemble into vertical periodic-amorphous organization. Such vertical order-disorder transition of colloidal particles is engineered by the evaporation process governed by the hydrophobicity of the substrate to reverse the pinning effect from "coffee-stain", heating temperature, and concentration of the colloidal particles. In the next step, the colloidal structure serves as a template to fabricate the final nanophotonic sensor.

The 2D fast Fourier transform of the SEM images shown in the inset indicates a short-range order of the top amorphous layer and periodic pattern at the bottom with a lattice of p = 370 nm. The optical resonance at normal incidence arises from the constructive interference of parallel crystal planes with lattice p following Bragg's law: $\lambda = 2pn^*$, where, λ being the resonant wavelength reflected from the nanophotonic cavity, n^* is the average refractive index of the cavity. The lattice and so the resonant wavelength depends on the diameter of the initial colloidal particles which is considered as 460 nm to produce reflection peaks at NIR (800 – 100 nm). Our hybrid design provides wide angle optical resonance around at 870 nm with resonance peak shift of 2 nm at 10° and 12 nm at 25° as shown in the Fig. 4. By contrast, the 3D periodic photonic crystal produced a 3-fold higher resonance shift of 38 nm at 25°. The finite-difference-time-domain (FDTD) simulations of both periodic and hybrid sensor support the experimental results as shown in Fig. 5. In addition, the intensity of periodic sensor decays considerably when the incident angle reached 20° due to the NA of the collection optics while the signal from the hybrid sensor remained detectable until 40° due to the wide-angle scattering from the amorphous pattern.

B. Sensor optomechanical properties and characterization

Nanophotonic silicone/PDMS is highly hydrophobic in nature, therefore aqueous humor does not penetrate into the nanoscale cavities and in turn the hydrostatic IOP deforms the cavity. At a given IOP, the sensor has an associated characteristic resonance peak wavelength. When the IOP increases, the flexible cavity is deflected inwards and causes the lattice p to decrease, and consequently results in a blue-shifted resonance. The location of these resonance peaks can be identified using a commercially available mini-spectrometer and used to determine the applied pressure, that is, the IOP.

The sensitivity of the sensor optomechanical response at the physiological range (0-40 mm Hg) depends on the softness or Young's Modulus, E of the flexible nanostructured material. To determine the proper material constraint, we modelled the displacement or deformation of the sensor under different pressure with finite element method in Fig. 6 and simulated the optomechnical sensitivity (peak wavelength shift vs applied pressure) for different E in Fig. 7. Any soft materials with E below 1 MPa is ideal for this application. We further engineered the E of silicone/PDMS by controlling the mixing ratio of base and curing agent and curing temperature as shown in Fig. 8.

We demonstrated benchtop optomechanical properties with 2 different materials: widely used Sylgard® with E = 0.4 and medical grade nuSil® with E = 1 MPa. We varied the pressure inside the chamber between 0 to 40 mm Hg using an integrated water column and a programmable syringe pump. A custom-built table-top detection system was used with broadband NIR light through an optically transparent window located in the lid of the chamber. The reflected optical resonance spectra from the sensor were then collected using a commercially available mini-spectrometer as shown in Fig. 9. As expected, Figs. 10 and 11 shows the blueshift of the resonance peak with increasing hydrostatic pressure for both kind of sensors. The sensitivity of the softer sensor is higher (0.4 nm/mm Hg) than the medical grade harder one (0.1 nm/mm Hg). Nevertheless, the medical grade hybrid sensor showed excellent linearity at the target IOP range when tested against a digital pressure gauge in Fig. 12. The maximum readout error was 0.56 mm Hg, 4-times better than most commercial tonometer (2 mm Hg).

C. In vivo sensor performance and IOP tracking

8 pre-calibrated medical grade sensors were implanted into the anterior chamber of eye through corneal incisions of 8 New Zealand white rabbits to investigate their performance *in vivo*. The sensors are visibly white and can be easily blended in with the iris without affecting the visual appearance (Fig. 13). We characterized the implanted sensors using a remote optical detector for up to 6 months at a high sampling rate of 10 Hz for 30s as shown in Fig. 14. When the reflected light is collected by the detector with perfect alignment within 10° field-of-view, it produces the highest SNR signals (>12 dB) and was chosen for IOP calculation to avoid potential error with alignment. Fig. 15 shows IOP measurements of three different sensors over the 6 months together with measured TonoVet data. The average IOP error of these three sensors (0.39 mm Hg) were lower than the TonoVet data (0.59 mm Hg). After six months of test studies, 7/8 sensors show good consistency with TonoVet with no sign of tissue buildup or inflammation.

III. CONCLUSION

We develop the smallest, passive and battery-free IOP sensor implant (Dia: 500 μm, Thick: 200 μm) which delivers IOP readings when simply interrogated with invisible, near-infrared light. The sensor is made of only a flexible medical-grade silicone structured with 3D photonic nanostructures functioning as a pressure-sensitive resonator with a sensitivity of 0.1 nm/mmHg. A new fabrication process is developed using colloidal self-assembly on a hydrophobic substrate as the template for the spongy structure. This process leads to a yet undescribed 3D hybrid photonic crystal (HPC) that combines periodic and amorphous morphology with almost no defects in the millimeter-scale. Such low index HPC results in a wide-angle resonant reflection (±40°) ensuring an easy remote readout. Finally, we demonstrated dynamic and long term changes of IOP in awake rabbits with an accuracy of 0.56 mm Hg over 0–40 mm Hg. With further sensor refinements and detector automation, it can become a viable choice for patient-initiated IOP and glaucoma management in the home environment.

REFERENCES

[1] H. A. Quigley, and T. B. Aimee, "The number of people with glaucoma worldwide in 2010 and 2020," *Br. J. Opt,* vol 90(3), pp. 262-267, 2006.

[2] H. A. Quigley, "Glaucoma," *Lanclet,* vol 377, pp. 1367-1377, 2011.

[3] I. Sanchez, and R. Martin, "Advances in diagnostic applications for monitoring intraocular pressure in Glaucoma: A review," *J. Opt.* vol 12(4), pp. 211-221, 2019.

[4] J. O. Lee, et al. "A microscale optical implant for continuous in vivo monitoring of intraocular pressure." *Micro. Nano.,* vol. 3, pp. 1-9, 2017.

[5] V. Narasimhan, et al. "Multifunctional biophotonic nanostructures inspired by the longtail glasswing butterfly for medical devices." *Nat. Nano.,* vol. 13.6, pp. 512-519, 2018.

[6] K. Y. Lee, et al. "Hydrophobic sponge structure‐based triboelectric nanogenerator." *Ad. Mat.,* vol. 26.29, pp. 5037-5042, 2014.

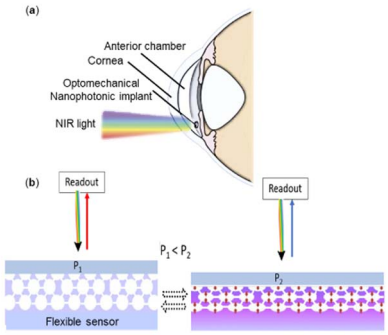

Fig. 1. (a) Nanophotonic intraocular pressure (IOP) sensor implanted in the anterior chamber and probed with NIR light. (b) Optomechanical operating principle of the sensor.

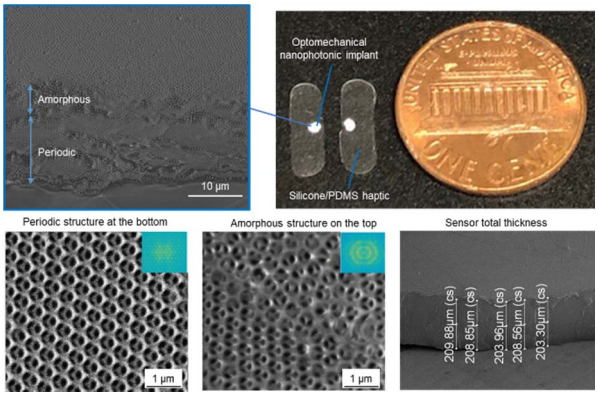

Fig. 2. A photograph of a completed device with a diameter of 500 µm. Scanning electron microscopy (SEM) images shows the hybrid periodic and amorphous nanopatterns and confirms the thickness of 200 um.

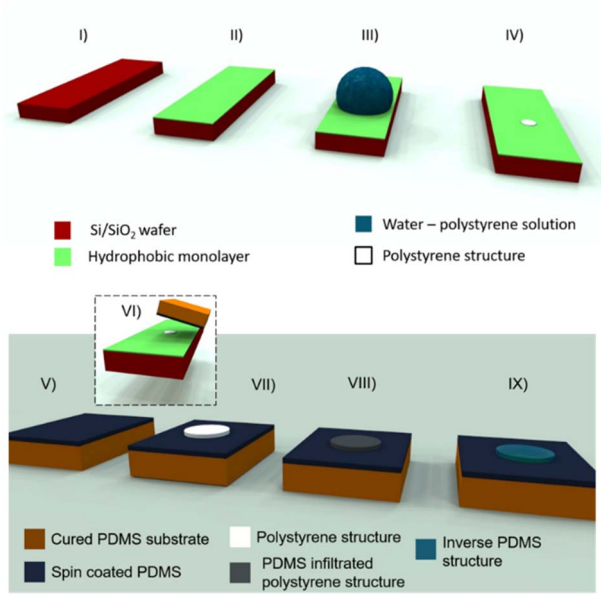

Fig. 3. Schematics of fabrication steps of the nanophotonic sensor.

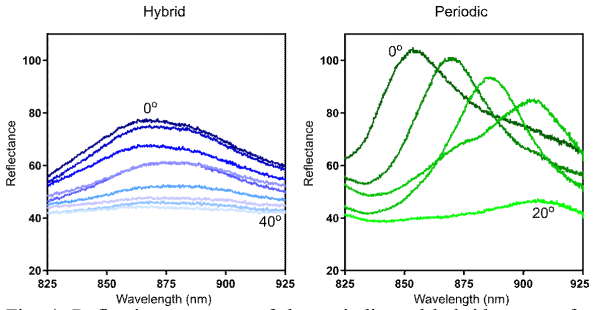

Fig. 4. Reflection spectrum of the periodic and hybrid sensors for different incident angles

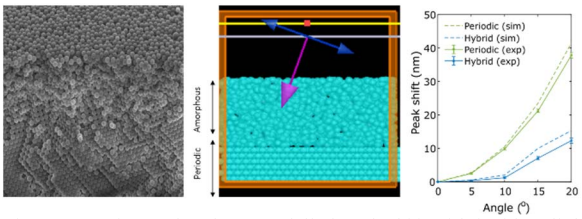

Fig. 5. Experimental and 3D modelled peak shift with incident light angle of both periodic and hybrid sensor

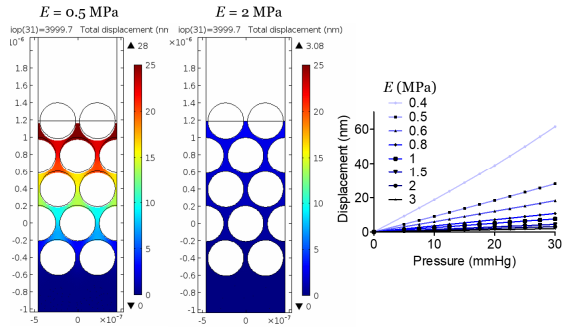

Fig. 6. FEM modeling of sensor displacement with applied pressure

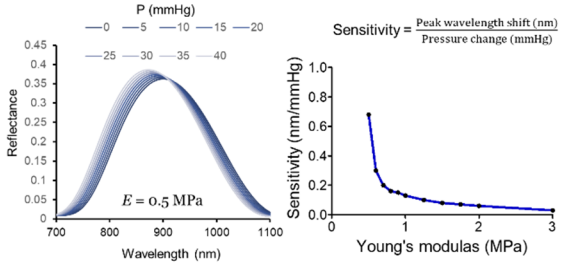

Fig. 7. Simulation of the optical response of the deformed sensor

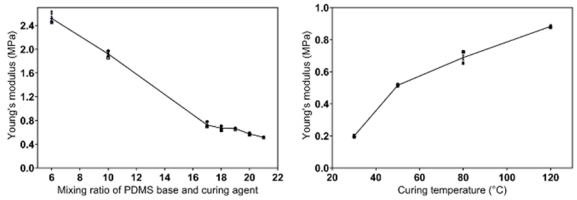

Fig. 8. Young's modulus modulation of the sensor material

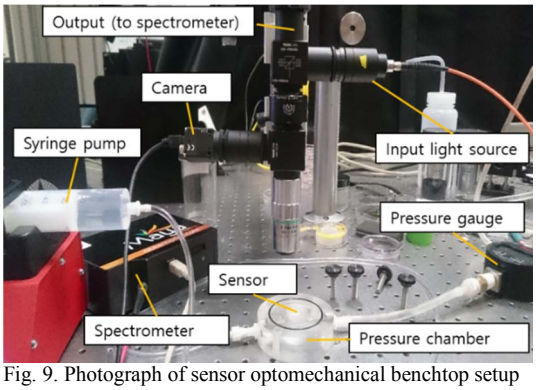

Fig. 9. Photograph of sensor optomechanical benchtop setup

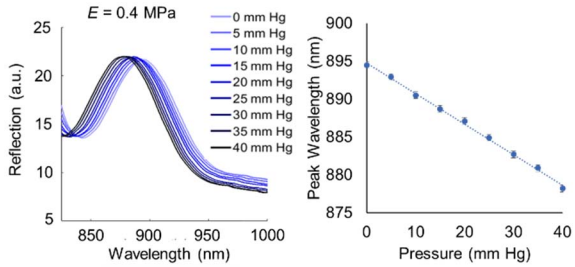

Fig. 10. Benchtop optomechanical response of softer sensor showing higher sensitivity of 0.4 nm/mm Hg (exp)/0.68 nm/mm Hg (sim)

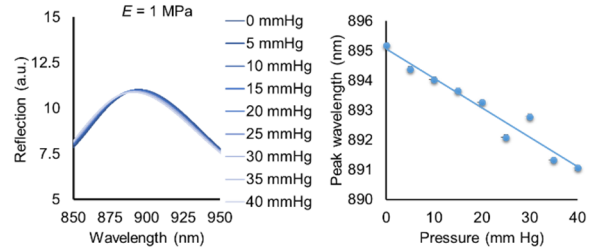

Fig. 11. Benchtop optomechanical response of harder sensor showing less sensitivity of 0.1 nm/mmHg (exp)/ 0.13 nm/mm Hg (sim)

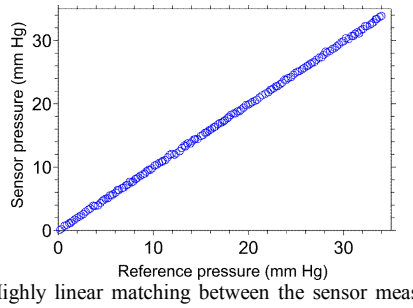

Fig. 12. Highly linear matching between the sensor measurements and the digital pressure-gauge readouts

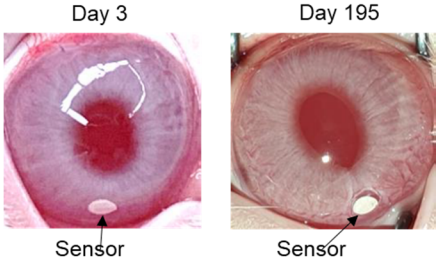

Fig. 13. Sensor (Rabbit 5) implanted in the eye after Day 3 and 195 showing no signs of tissue buildup

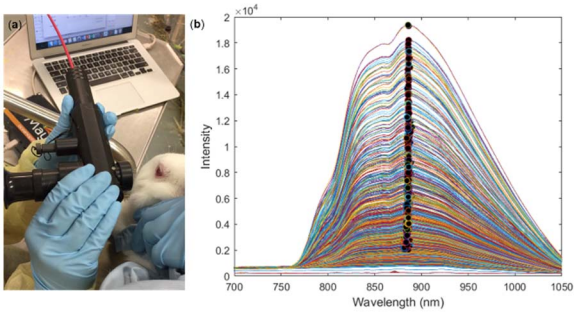

Fig. 14. (a) Handheld measurement setup and (b) *in vivo* spectra with peak detection from 30s remote detector measurement at 10 Hz.

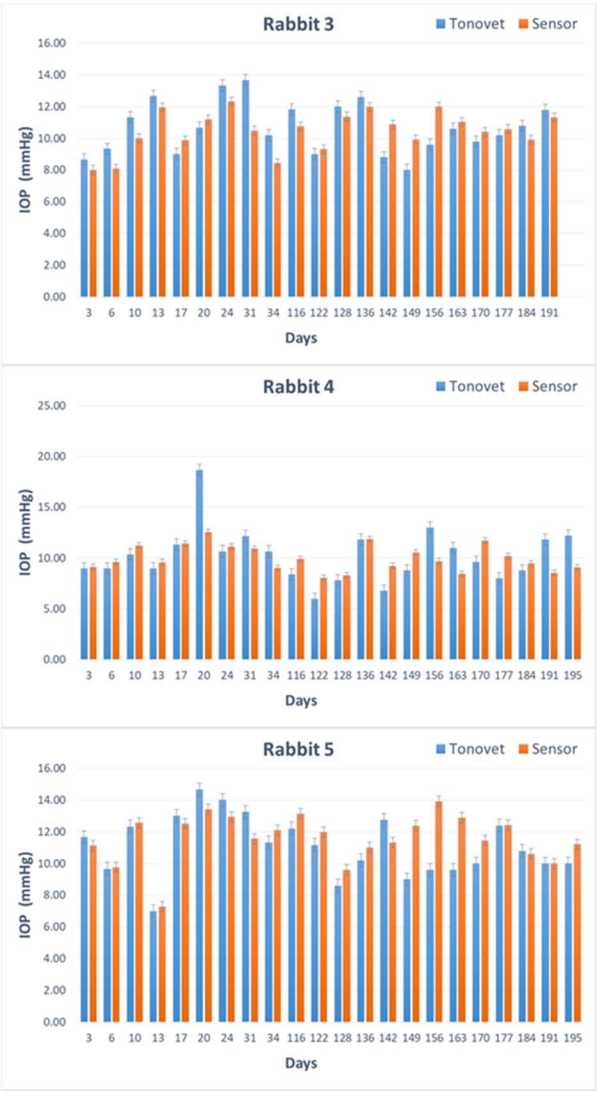

Fig. 15. Comparison of IOP derived from 3 implanted sensor measurements vs TonoVet IOP measurements over a 191-day period.